Journal of Hazardous Materials 478 (2024) 135375

Contents lists available at ScienceDirect

Journal of Hazardous Materials

journal homepage: www.elsevier.com/locate/jhazmat

1,2-bis(2,4,6-tribromophenoxy) ethane induces necroptosis via the co-competition of GAS5 and NUAK1 for miR-743a-5p in rat hepatocytes

Yuan Cui [a,b], Qianqian Xiao [a,b], Qiong Zhang [a,b], Jiawei Yang [a,b], Yuetong Liu [a,b], Weidong Hao [a,b], Jianjun Jiang [a,b], Qinghe Meng [a,b], Xuetao Wei [a,b,*]

[a] Department of Toxicology, School of Public Health, Peking University, Beijing 100191, PR China
[b] Beijing Key Laboratory of Toxicological Research and Risk Assessment for Food Safety, Beijing 100191, PR China

HIGHLIGHTS

- The mechanism of BTBPE hepatotoxicity has been explored from perspective of ceRNA for the first time.
- BTBPE caused necroptosis in liver and BRL cells.
- NUAK1 was a newly discovered upstream regulatory target for necroptosis.
- miR-743a-5p was found for the first time to inhibit necroptosis by targeting NUAK1 and down-regulating NUAK1.
- The GAS5-miR-743a-5p-NUAK1 axis is involved in the regulation of necroptosis in the form of ceRNA for the first time.

GRAPHICAL ABSTRACT

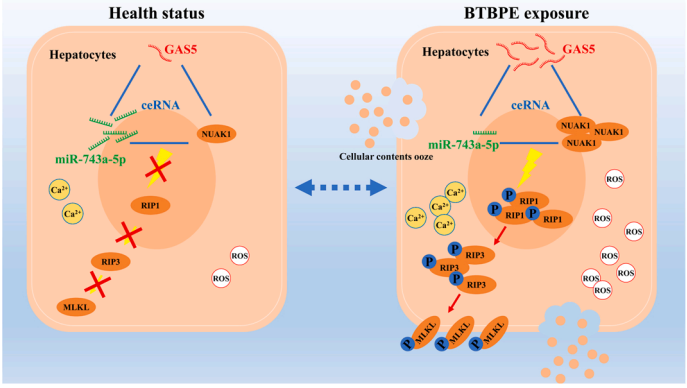

ARTICLE INFO

Keywords:
BTBPE
Necroptosis
GAS5
MiR-743a-5p
NUAK1
Liver

ABSTRACT

The brominated flame retardant 1,2-bis(2,4,6-tribromophenoxy) ethane (BTBPE) widely used in manufacturing is inevitably released into the environment, resulting in the exposure of organisms to BTBPE. Therefore, it is particularly important to explore its toxic mechanism. The liver is one of the main accumulating organs of BTBPE, but the mechanism underlying BTBPE hepatotoxicity has not been thoroughly investigated. In our study, BTBPE was administered to Sprague–Dawley (SD) rats and rat hepatocytes (BRL cells) in vivo and in vitro, respectively, and HE staining, AO/EB staining, fluorescent probes, qPCR, immunofluorescence, and dual-luciferase reporter assays were performed. We investigated the mechanism of action of growth arrest-specific 5 (GAS5), miR-743a-5p, and NUAK family kinase 1 (NUAK1) in BTBPE-induced necroptosis from the perspective of competing endogenous RNAs (ceRNAs) using NUAK1 inhibitors, siRNAs, mimics, and overexpression plasmids. Our study showed that exposure to BTBPE caused necroptosis in the liver and BRL cells, accompanied by an oxidation-reduction imbalance and an inflammatory response. It is worth noting that NUAK1 is a newly discovered upstream regulatory target for necroptosis. In addition, miR-743a-5p was shown to inhibit necroptosis by targeting NUAK1 and down-regulating NUAK1. GAS5 upregulates NUAK1 expression by competitively binding to miR-743a-5p, thereby inducing necroptosis. This study demonstrated, for the first time, that the

* Corresponding author at: Department of Toxicology, School of Public Health, Peking University, Beijing 100191, PR China.
E-mail address: weixt@bjmu.edu.cn (X. Wei).

https://doi.org/10.1016/j.jhazmat.2024.135375
Received 7 May 2024; Received in revised form 15 July 2024; Accepted 27 July 2024
Available online 29 July 2024

GAS5-miR-743a-5p-NUAK1 axis is involved in the regulation of necroptosis via ceRNAs. Thus, GAS5 and NUAK1 induce necroptosis by competitively binding to miR-743a-5p.

1. Introduction

Brominated flame retardants are widely used in electronic products, textiles, furniture, and other commodities and are released into the environment and harm the health of organisms [1]. Novel brominated flame retardants can enter the body through the digestive and respiratory tracts, and have been shown to have potential biological toxicity and accumulative effects [2]. 1,2-bis(2,4,6-tribromophenoxy) ethane (BTBPE) is a new type of brominated flame retardant that is widely distributed in water, soil, sediments, and indoor and outdoor atmospheres. The BTBPE content in sewage can reach 20.2 ng/L [3]. In biological sludge, the BTBPE can reach 1226.8 ng/g [3]. The concentration of BTBPE in the atmosphere in South Korea is as high as 1000 ng/g dw [4]. In addition, in UK car interior dust, the BTBPE content can reach 120 ng/g [5]. According to the test results of 111 breast milk samples donated by 37 healthy mothers in Beijing, the concentration of BTBPE in breast milk was 2.56 ng/g lw [6]. Theoretically, the occupational population will be exposed to higher concentrations of BTBPE, and high exposure and cumulative effects will exacerbate BTBPE harm to the body. However, there is currently a lack of exposure information for BTBPE occupational groups. Exposure to BTBPE can cause oxidative stress and mitochondrial damage, which can impair immune, endocrine, and reproductive functions [7–9]. In addition, some studies and our laboratory research have found that BTBPE is toxic to the thyroid [10, 11]. Our laboratory has also found that BTBPE damages the intestinal barrier by damaging tight junctions and inhibiting mucus secretion [12]. Importantly, in-depth research on the mechanism of hepatotoxic action of BTBPE is lacking.

The cell fate directly affects the health of an organism. In a healthy state, cells replace old and new cells via apoptosis, which is usually not accompanied by inflammation and maintains homeostasis of the internal environment and health [13]. However, when the body receives external environmental stimuli such as bacteria, viruses, toxic substances, and radiation, cells die in various ways, including pyroptosis, ferroptosis, excessive autophagy, and necroptosis [14–17]. These other forms of cell death are usually accompanied by the release of cell contents, and the production of large amounts of oxidative products and inflammatory factors [18,19]. Necroptosis is a type of programmed cell death commonly observed in various pathological states. When cells are exposed to harmful stimuli, the expression levels of receptor-interacting serine/threonine-protein kinase 1 (RIP1), receptor-interacting serine/threonine-protein kinase 3 (RIP3), mixed lineage kinase domain-like (MLKL) proteins, and their phosphorylated proteins increase, accompanied by increased levels of reactive oxygen species (ROS) and cytoplasmic calcium ions. In addition, the production of inflammatory factors is increased, cell contents leak, and significant inflammation is usually observed in vivo [12]. Necroptosis caused by different factors has the same regulatory mechanism, but different initiation mechanisms. At present, there are still many gaps in the research on the regulation of necroptosis by non-coding RNA. Previous studies have found that NUAK family kinase 1 (NUAK1) is associated with biological processes such as response to glucose starvation, regulation of myosin light chain phosphatase activity, synaptic function, tumor formation, cell adhesion, and cell aging [20–23]. NUAK1 has p53 binding activity and protein serine/threonine kinase activity [24,25]; however, there is currently no research on the relationship between NUAK1 and necroptosis.

Recent studies have shown that less than 2 % of the total genome is composed of protein-coding genes, indicating that non-coding RNA account for most of the human transcriptome [26]. Recently, popular areas in non-coding RNAs research have included microRNAs (miRNAs), pseudogenes (Ψ), long non-coding RNA (lncRNA), and circular RNA (circRNA) [27]. Non-coding RNAs have been shown to be involved in a wide range of biological processes, such as cell fate programming, aging, and disease [28–30]. lncRNAs range in length from 200 nucleotides to 100 kb and are associated with a variety of biological processes. Although thousands of lncRNAs have been identified over the last few decades, only a small number have been functionally characterized [26]. miRNAs are well-known post-transcriptional regulators; however, in recent years, miRNAs, as information media, have been shown to interact with many different types of RNA molecules to establish a homeostasis balance between transcriptional products [31]. A classic example of RNA-RNA interactions is the post-transcriptional regulation of RNA transcripts by miRNAs [26]. As researchers continue to understand the transcriptome space, a hypothesis has emerged that numerous miRNA binding sites are present on various RNA transcripts, and all RNA transcripts containing miRNA binding sites can interact and regulate each other through specific competition for shared miRNAs, thereby acting as competing endogenous RNAs (ceRNAs) [26]. lncRNAs usually act upstream of the ceRNA regulatory relationships, and miRNAs often act as bridges between mRNA and lncRNAs, which together form a ceRNA regulatory network. lncRNAs mainly weaken the activity of miRNAs through the targeted binding of sites to upregulate target genes regulated by miRNAs [32]. Research on how ceRNAs regulate necroptosis is limited. In this study, we focused on lncRNA growth arrest-specific 5 (GAS5). Based on the information provided in the database (LncRNADisease v3.0), we found a strong correlation between GAS5 and non-alcoholic fatty liver disease (score: 0.985791), as shown in Fig. 1A and B, which is consistent with our research objectives. In addition, GAS5 was associated with diabetic cardiomyopathy, renal fibrosis, cerebral infarction, and other diseases, as shown in Fig. 1C and D. However, there are currently no studies on the relationship between GAS5 expression and necroptosis.

The liver is one of the main accumulating organs of BTBPE, and the mechanism of BTBPE hepatotoxicity has not been thoroughly investigated[7,33]. This study considered the hepatotoxicity of BTBPE as a starting point, and found that BTBPE induced necroptosis in rat hepatocytes. Moreover, the mechanism of BTBPE-induced necroptosis was explored from the perspective of ceRNAs, and GAS5 and NUAK1 were found to regulate necroptosis through co-competition with miR-743a-5p. This study is the first to identify a relationship between NUAK1 and necroptosis. We discovered that the GAS5-miR-743a-5p-NUAK1 axis is involved in necroptosis. This study enriches our understanding of the mechanisms underlying the liver damage caused by BTBPE exposure, provides new directions for the study of necroptosis, and identifies the biological functions of GAS5, miR-743a-5p, and NUAK1.

2. Materials and methods

2.1. Animals and cell treatments

BTBPE (CAS: 37853–59-1, purity $\geq$ 98 %) was purchased from AccuStandard Inc. (New Haven, CT, USA). Sprague–Dawley (SD) rats were raised in a specific pathogen-free barrier system. A total of 48 healthy male SD rats aged 6–7 weeks were randomly divided into four groups. The in vivo experimental dose was calculated based on the daily human exposure dose and safety factor. The control (NC), low-dose (L), medium-dose (M), and high-dose (H) groups were orally administered BTBPE at 0, 2.5, 25, and 250 mg/kg/day, respectively, once daily for one month. All animal procedures were approved by the Animal Welfare and Ethics Inspection Committee of Peking University and were

performed in accordance with the governmental Guidelines for the Care and Use of Laboratory Animals.

In the in vitro studies, BTBPE was dissolved in DMSO to different concentrations of the mother liquor, which was then diluted again to the desired final concentration using a medium. BTBPE at 0 μM (NC group), 5 μM (L group), 10 μM (M group), and 20 μM (H group) was used to treat rat hepatocytes (BRL cells, BeNa Culture Collection, BNCC338493) for 24 h. BRL cells were cultured in 90 % DMEM (Thermo Fisher Scientific Inc., USA) and 10 % fetal bovine serum (Cellmax, Beijing, SA201.01). The BTBPE group was treated with 20 μM BTBPE, the HTH group was treated with 1 μM HTH-01–015 (HY-12334, MCE Company, HTH), HTH+BTBPE group given 20 μM BTBPE and 1 μM HTH, the miR-743a-5p mimic group was transfected with 100 pmol mimic per well, the miR-743a-5p mimic+BTBPE group was transfected with 100 pmol mimic per well and treated with 20 μM BTBPE, the si-GAS5 group was transfected with 100 pmol siRNA per well (siRNA sequence of GAS5 is shown in Table S1), the si-GAS5 +BTBPE group was transfected with 100 pmol siRNA per well and treated with 20 μM BTBPE, the OE-NUAK1 group and OE-GAS5 group was transfected with 1 μg recombinant plasmid per well, and the miR-743a-5p mimic+OE-NUAK1 group and miR-743a-5p mimic+OE-GAS5 group were transfected with 1 μg recombinant plasmid and 100 pmol mimic per well. The pcDNA3.1 plasmid was used to overexpress GAS5 and NUAK1. The transfection time was 12 h.

2.2. Hematoxylin and eosin staining

The liver tissue was fixed in 4 % paraformaldehyde. Subsequently, dehydration, embedding, slicing, and hematoxylin and eosin (HE) staining were performed [34]. Histopathological observations were performed using a vertical light microscope and images were obtained using an M8 digital scanning microscope imaging system (Precipitate Point, Bavaria, Germany) (n = 3).

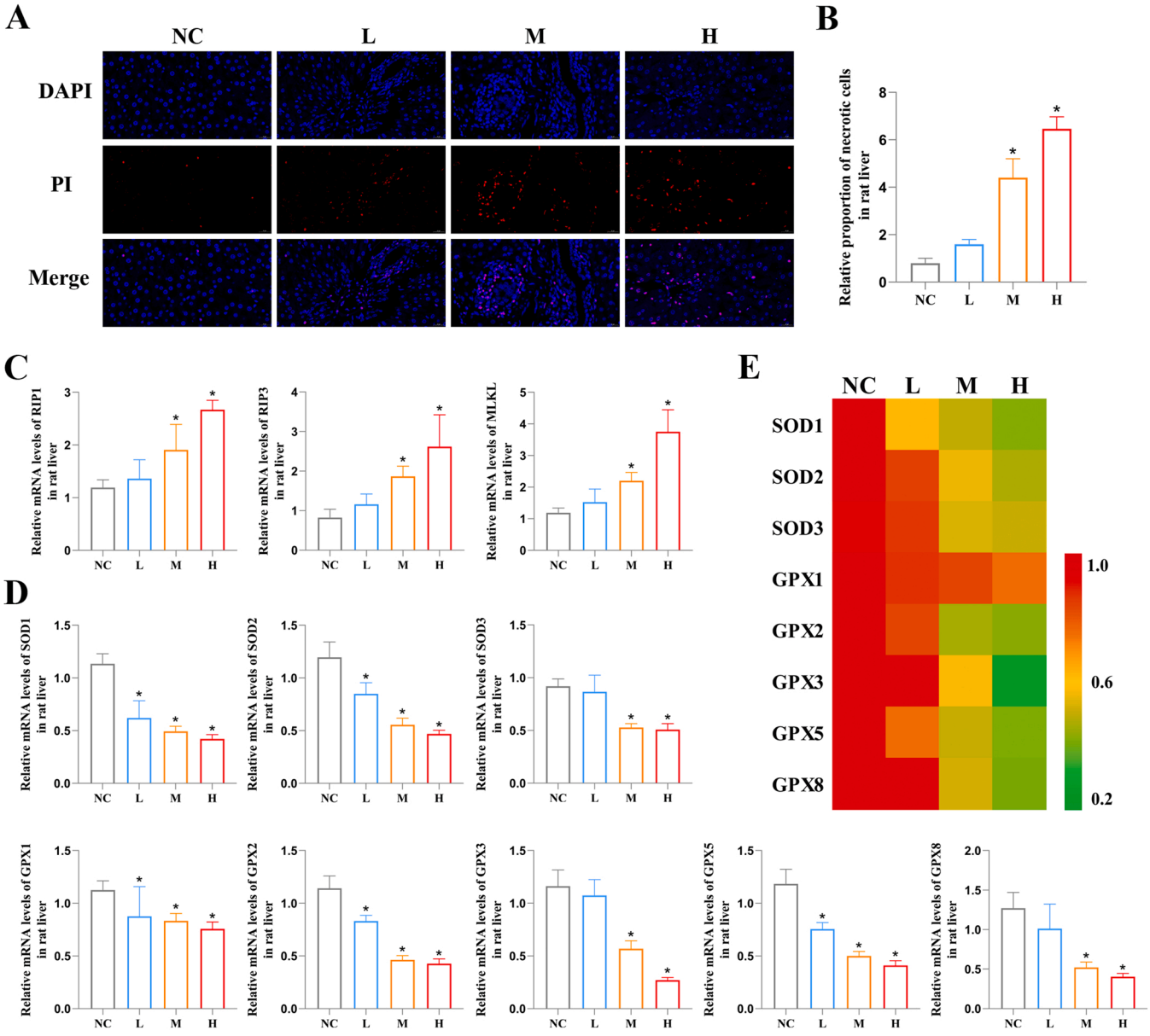

Fig. 1. BTBPE induces necroptosis in rat liver. (A) PI staining images in liver after BTBPE exposure. (B) Relative proportion of necrotic cells in liver after BTBPE exposure. (C) The mRNA levels of RIP1, RIP3 and MLKL in liver after BTBPE exposure. (D) The mRNA levels of antioxidant enzyme-related genes in liver after BTBPE exposure. (E) Heatmap to analyze the mean values of the antioxidant enzyme-related gene PCR quantification results in liver after BTBPE exposure. All experiments were repeated at least three times (n ≥ 3). Results are expressed as mean ± standard deviation. The asterisk represents a significant difference compared to the NC group or between different groups (*$P < 0.05$).

2.3. ELISA assay

The liver was prepared into 10 % tissue homogenate. The kit (Nanjing Jiancheng, Bioengineering Institute, PR China) detected the content of interleukin 4 (IL4), interleukin 6 (IL6) and interferon γ (IFNγ) in rat liver. The absorbance of each hole was measured by multifunctional microplate reader (BMG Labtech FLUOstar Omega, Germany).

2.4. Propidium iodide staining

The liver tissue was fixed in 4 % paraformaldehyde. Subsequently, slicing, dewaxing with water, drawing circles, PI staining of the nuclei, and sealing with an anti-fluorescence quenching agent were performed. Images were captured using a fluorescence microscope (IX53; Olympus Corporation, Tokyo, Japan) (n = 3).

2.5. AO/EB staining

An acridine orange/ethidium bromide (AO/EB) staining kit (Sangon Biotech Co., Ltd., China) was used to detect necrotic cells. After treatment, the medium was discarded and the cells were washed with PBS. AO and EB staining solutions were added and images were observed under a fluorescence microscope after staining for 5 min (n = 3). After AO/EB staining, normal cells appeared green and necrotic cells appeared orange or orange-red.

2.6. Antioxidant ability and ROS assay

The liver was prepared into 10 % tissue homogenate. Antioxidant capacity was assessed using kits to determine reduced glutathione (GSH) and superoxide dismutase (SOD) levels according to the manufacturer's instructions (Jiangsu Meimian Industrial Co. Ltd.(Jiangsu,China)). The absorbance of each hole was measured by multifunctional microplate reader.

A DCFH-DA probe (Wanlei Biological Company, China; WLA131) was used to detect the ROS levels in BRL cells. After treatment, the medium was discarded and the cells were washed with PBS. BRL cells were incubated with DCFH-DA probes diluted 1000 times in culture medium for 30 min in a 37 ℃ incubator. The DCFH-DA probe does not exhibit fluorescence. When the DCFH-DA probe enters the cell, it is hydrolyzed to DCFH, which is then oxidized to a green fluorescent substance by ROS[35]. Excess DCFH-DA probes were washed with PBS and examined by flow cytometry (Beckman Coulter FC500-MPL) (n = 3).

2.7. Cytoplasmic calcium ion staining

A Fluo-4 AM probe (Beyotime Biotechnology, Shanghai, China) was used to detect cytoplasmic calcium levels. Fluo-4 AM is cleaved by intracellular esterases to form Fluo-4, which binds calcium ions and produces strong green fluorescence. After treatment, the medium was discarded and the cells were washed with PBS. Fluo-4 working solution was added and the cells were incubated in dark at 37 ℃ for 30 min, then observed using a fluorescence microscope (n = 3).

2.8. Dual luciferase reporter assay

A recombinant plasmid was constructed based on the pMIR-Glo vector. Sequences near the target binding sites between the 3′ UTR region of NUAK1 or GAS5 and miR-743a-5p were inserted into the vector. The recombinant plasmids were named pMIR-GAS5 and pMIR-NUAK1, respectively. The sequences of pMIR-GAS5 and pMIR-NUAK1 are listed in Table S2. BRL cells were transfected with 750 ng of pMIR-GAS5 or pMIR-NUAK1 and 100 pmol of the miR-743a-5p mimic. Lipofectamine 2000 reagent was used for cell transfection. Dual luciferase reporter assay was performed using Dual Luciferase®Reporter Assay System (Promega). Luciferase activity was measured using a multifunctional microplate reader (n = 3).

2.9. Total RNA isolation and real-time quantitative PCR analysis

Total RNA was isolated from the liver and BRL cells of each group using TRIzol reagent (TransGen Biotech, Beijing, China). The reverse transcription of cDNA was performed according to the manufacturer's instructions (SPARKscript 1st Strand cDNA Synthesis Kit (with gDNAEraser) (Shandong Sparkjade Biotechnology Co., Ltd.)). SYBR Green (K1070, APExBIO, Houston, USA) was used for the qRT-PCR (n = 6)[36]. β-actin was used as an internal reference gene. U6 was used as the internal reference gene for miRNA. The primers used for gene detection are listed in Table S3.

2.10. Immunofluorescence

The BRL cells were treated as described above and fixed with paraformaldehyde. After removing paraformaldehyde, the sample was sealed with a sealing solution for 60 min. After the sealing solution was removed, and diluted specific primary antibody was used overnight at 4 ℃. After removing the primary antibody, the diluted fluorescently labeled secondary antibody was added and incubated in the dark for 60 min. The secondary antibody was recovered, and antifade mounting medium with DAPI (Beyotime Biotechnology) was added[37]. Fluorescence images were obtained using a fluorescence microscope. ImageJ software was used to analyze relative fluorescence intensity (n = 3). The dilutions of the primary antibodies were as follows: RIP1 (Bioss, USA) 1:100, pRIP3 (CST, USA) 1:1000, and pMLKL (CST, USA), 1:1000.

2.11. Statistical analysis

Statistical analysis was performed using one-way analysis of variance (ANOVA) in SPSS 24.0. All experiments were repeated at least three times (n ≥ 3). Results are expressed as mean ± standard deviation. The asterisk represents a significant difference compared to the NC group or between different groups (* $P < 0.05$). Spearman's rank correlation analysis was used to investigate the relationships between the levels of all detected genes.

3. Results

3.1. BTBPE induces necroptosis in rat liver

After BTBPE exposure, the rat livers were stained with PI. The PI stains dead cells red. As the BTBPE exposure dose increased, the number of dead cells gradually increased, as shown in Fig. 1A and B. Subsequently, the mRNA levels of necroptosis markers were detected, as shown in Fig. 1C. The results showed that as the dose of BTBPE increased, the gene expression levels of RIP1, RIP3, and MLKL gradually increased. An imbalance in redox state is accompanied by necroptosis. Therefore, we examined the gene expression of several antioxidant enzymes (Fig. 1D). The average expression levels of the antioxidant enzyme genes were characterized using a heatmap (Fig. 1E). The gene expression levels of several antioxidant enzymes were significantly reduced in the M and H groups. Then, we examined the SOD and GSH levels in liver (SFig. 1E and F). The GSH and SOD levels were significantly reduced in the M and H groups. These results indicate that BTBPE exposure induces necroptosis in rat liver.

3.2. BTBPE induces inflammation in rat liver

HE staining showed inflammatory cell infiltration in the liver after BTBPE exposure, which was particularly evident in the H group (Fig. 2A). Subsequently, the expression levels of 16 inflammation-related genes were determined and the average expression levels were

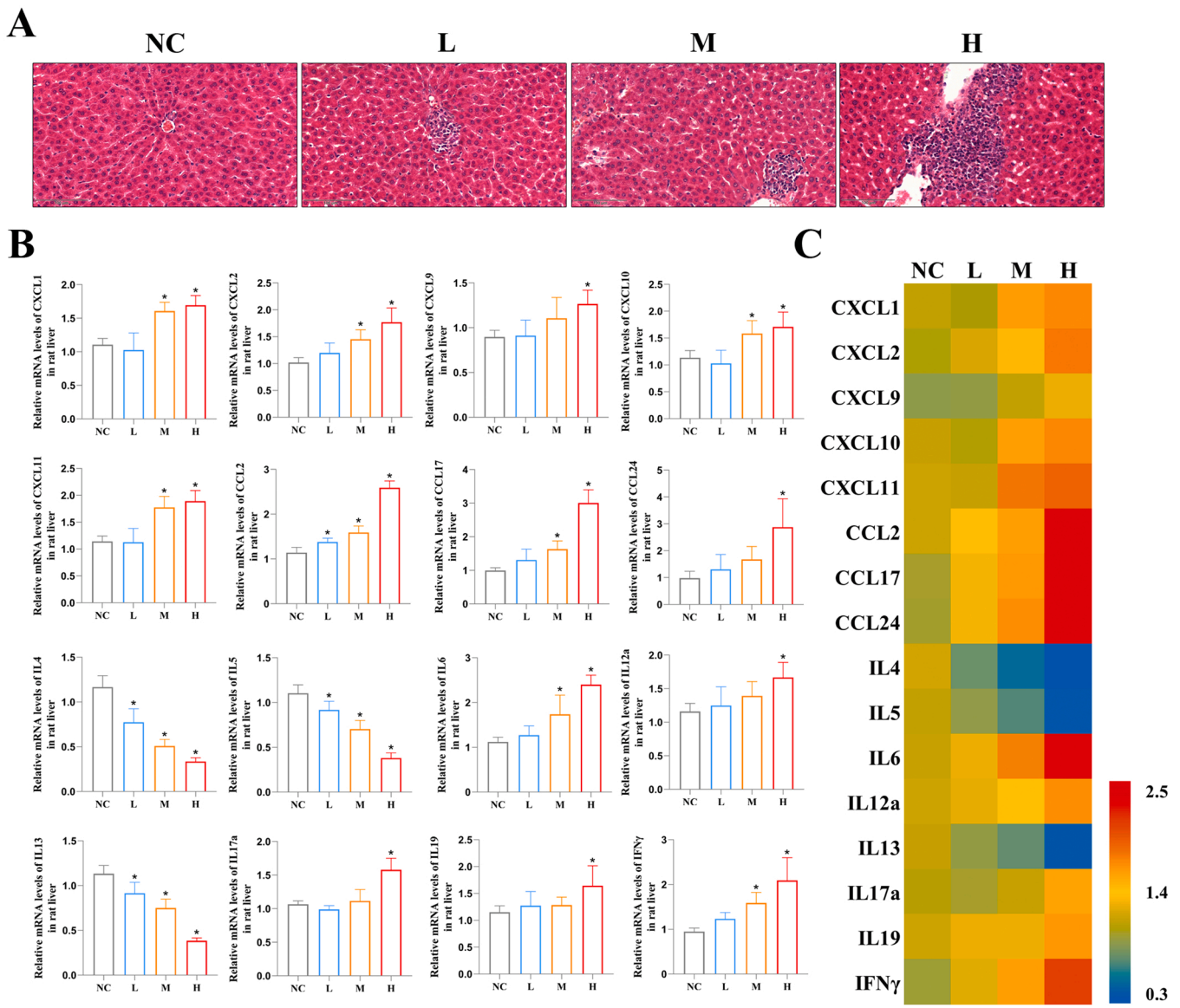

Fig. 2. BTBPE induces inflammation in rat liver. (A) HE staining images in liver after BTBPE exposure. (B) mRNA levels of inflammatory-related genes in liver after BTBPE exposure. (C) Heatmap to analyze the mean values of the inflammatory-related gene PCR quantification results in liver after BTBPE exposure. All experiments were repeated at least three times (n ≥ 3). Results are expressed as mean ± standard deviation. The asterisk represents a significant difference compared to the NC group or between different groups (*$P < 0.05$).

characterized using a heatmap (Fig. 2B and C). In the M group, most inflammatory genes showed significant changes, whereas in the H group, all genes showed significant changes. Then, we examined the IL4, IL6 and IFNγ levels in liver (SFig. 1 G-I). The IL4 level were significantly reduced in the M and H groups. The IL6 and IFNγ levels were significantly increased in the M and H groups. These results indicate that BTBPE exposure induces inflammation in rat liver.

3.3. BTBPE induces necroptosis in BRL cells

To further verify the necroptotic effects of BTBPE, we used BRL cells. The results showed that as the dose of BTBPE increased, the gene expression levels of RIP1, RIP3, and MLKL gradually increased (Fig. 3A-C). The AO/EB staining results also showed that the relative proportion of necrotic cells gradually increased with increasing BTBPE dose (Fig. 3D and E). Next, we used immunofluorescence to detect the relative protein levels of RIP1, pRIP3, and pMLKL (Fig. 2A and B, Fig. 3F and G, and Fig. 3H and I, respectively). As the exposure dose of BTBPE increased, the relative fluorescence intensities of RIP1, pRIP3, and pMLKL gradually increased.

Increased cytoplasmic calcium and ROS levels are the concomitant effects of necroptosis. The Fluo-4 AM probe was used to detect calcium ion levels in BRL cells, and the green fluorescence intensity represented the cytoplasmic calcium ion level (Fig. 3J and K). As the BTBPE dose increased, the calcium ion levels in BRL cells gradually increased. A DCFH-DA probe was used to detect ROS levels in BRL cells (Fig. 3L and M). As the exposure dose of BTBPE increased, the levels of ROS in BRL cells gradually increased. These results indicate that BTBPE causes necroptosis in BRL cells.

3.4. Both NUAK1 and GAS5 are target genes for miR-743a-5p

In the livers of the M and H groups, the gene expression levels of NUAK1 and GAS5 were significantly increased (Fig. 4A and B). Similarly, in BRL cells, BTBPE exposure significantly increased the gene expression levels of NUAK1 and GAS5 (Fig. 4D and E). We predicted the

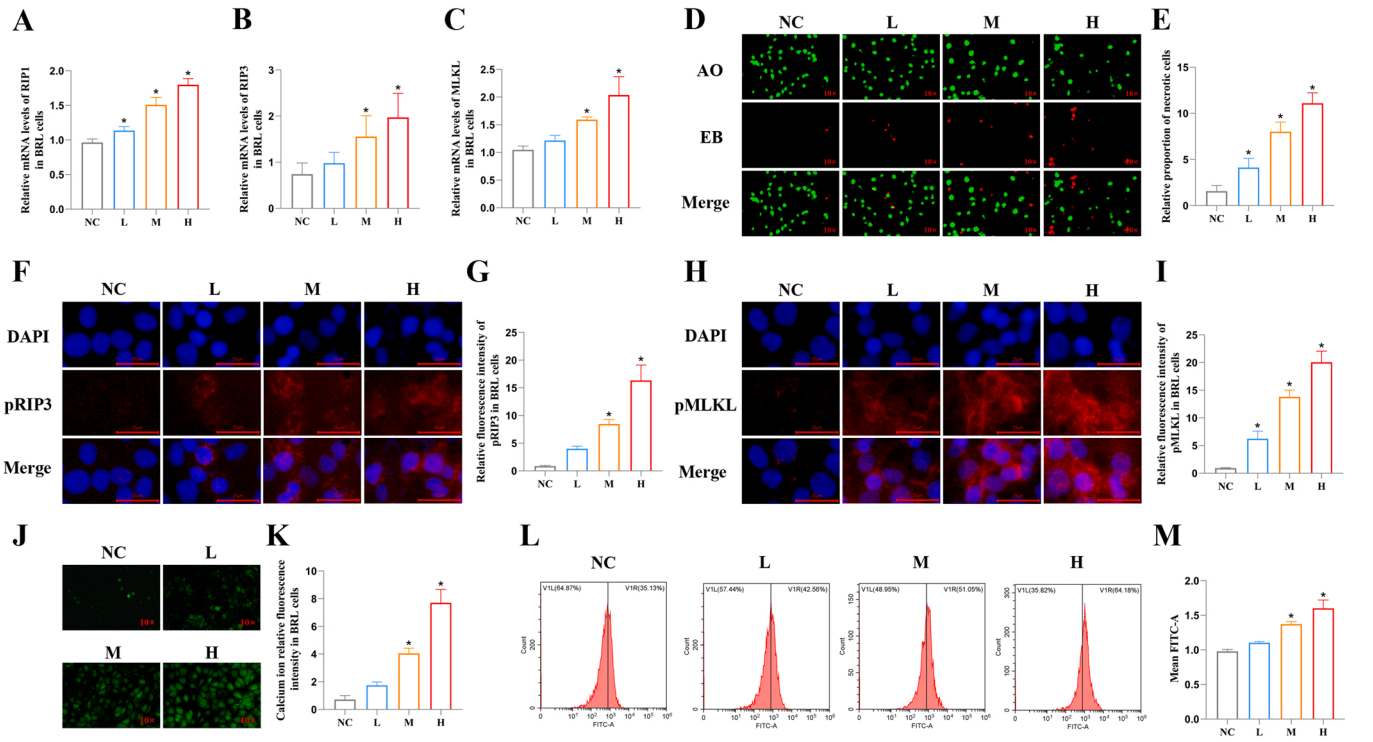

Fig. 3. BTBPE induces necroptosis in BRL cells. (A) The mRNA level of RIP1 in BRL cells after BTBPE exposure. (B) The mRNA level of RIP3 in BRL cells after BTBPE exposure. (C) The mRNA level of MLKL in BRL cells after BTBPE exposure. (D) Effects of BTBPE on BRL cells necrosis by AO/EB staining. After AO/EB staining, the normal cells appeared green, and the necrotic cells appeared orange or orange-red. (E) Relative proportion of necrotic cells after BTBPE exposure. (F) Effects of BTBPE on protein level of pRIP3 in BRL cells analyzed using immunofluorescence. (G) pRIP3 relative fluorescence intensity after BTBPE exposure in BRL cells. (H) Effects of BTBPE on protein level of pMLKL in BRL cells analyzed using immunofluorescence. (I) pMLKL relative fluorescence intensity after BTBPE exposure in BRL cells. (J) Effects of BTBPE on level of cytoplasmic calcium ion in BRL cells analyzed using Fluo-4 probe. (K) Cytoplasmic calcium ion relative fluorescence intensity after BTBPE exposure in BRL cells. (L) Effects of BTBPE on level of ROS in BRL cells analyzed using DCFH probe. (M) ROS relative level in BRL cells after BTBPE exposure. All experiments were repeated at least three times ($n \geq 3$). Results are expressed as mean ± standard deviation. The asterisk represents a significant difference compared to the NC group or between different groups (*$P < 0.05$).

target miRNAs of NUAK1 and GAS5 using the miRDB database (https://mirdb.org/), and identified a common target miRNA, miR-743a-5p. Next, we measured the expression levels of miR-743a-5p in the liver and BRL cells. With the increase of the BTBPE dose, the expression levels of miR-743a-5p gradually decreased (Fig. 4C and F). Using bioinformatics methods, we discovered the binding sites of miR-743a-5p in 3′UTR of NUAK1 and GAS5 (Fig. 4G), indicating that the two had the same binding site. To determine the targeting relationship between NUAK1, GAS5, and miR-743a-5p, we performed dual-luciferase reporter assays. After miR-743a-5p mimic treatment, luciferase activity in the two experimental groups was significantly reduced (Fig. 4H and I), indicating that miR-743a-5p had targeting relationships with NUAK1 and GAS5. These results indicated that NUAK1 and GAS5 are both target genes of miR-743a-5p and exhibit negative regulatory relationships.

3.5. *Inhibiting NUAK1 alleviates necroptosis induced by BTBPE in BRL cells*

To investigate the mechanism of the coding gene NUAK1 in BTBPE-induced necroptosis, we used HTH, a potent NUAK1 inhibitor. First, AO/EB staining results showed that, compared with the NC group, the proportion of necrotic cells in the BTBPE group was significantly increased, whereas in the HTH+BTBPE group, it was significantly decreased compared with the BTBPE group (Fig. 5A and B). Further experiments showed that HTH reduced the increased gene expression levels of RIP1, RIP3, and MLKL induced by BTBPE (Fig. 5C-E). Similarly, the BTBPE-induced increase in RIP1, pRIP3, and pMLKL protein levels was significantly inhibited by HTH (Fig. 2C and D, Fig. 5F and G, and Fig. 5H and I). Cytoplasmic calcium ion and ROS levels were measured (Fig. 5J-M). Cytoplasmic calcium ion and ROS BTBPE group were significantly higher than those in the NC group. Compared to the BTBPE group, the levels of cytoplasmic calcium ions and ROS in the HTH+BTBPE group were significantly reduced. These results indicate that HTH can inhibit BTBPE-induced necroptosis in BRL cells and the accompanying increase in cytoplasmic calcium ions and ROS levels. Thus, NUAK1 is involved in the upstream regulation of necroptosis.

3.6. *miR-743a-5p alleviates necroptosis induced by BTBPE in BRL cells*

Subsequently, miR-743a-5p mimics were used to investigate the upstream regulatory mechanisms of NUAK1. As shown in Fig. 6A, the level of miR-743a-5p significantly increased in cells transfected with the miR-743a-5p mimic. Compared with the BTBPE group, the level of NUAK1 in the miR-743a-5p mimic+BTBPE group was significantly reduced (Fig. 6B), suggesting that overexpression of miR-743a-5p in cells could effectively inhibit NUAK1.

AO/EB staining showed that the proportion of necrotic cells in the BTBPE group was significantly increased compared to that in the NC group, whereas that in the miR-743a-5p mimic+BTBPE group was significantly reduced compared to that in the BTBPE group (Fig. 6 C and D). Further experiments showed that the miR-743a-5p mimic reduced the elevated mRNA levels of RIP1, RIP3, and MLKL induced by BTBPE (Fig. 6E-G). Similarly, the miR-743a-5p mimic significantly inhibited the BTBPE-induced increases in RIP1, pRIP3, and pMLKL protein levels (Fig. 3A and B, Fig. 6H and I, and Fig. 6 J and K). Cytoplasmic calcium ions and ROS levels were then measured (Fig. 6L-O). Cytoplasmic calcium ion and ROS BTBPE group were significantly higher in those in the NC group. Compared to the BTBPE group, the levels of cytoplasmic

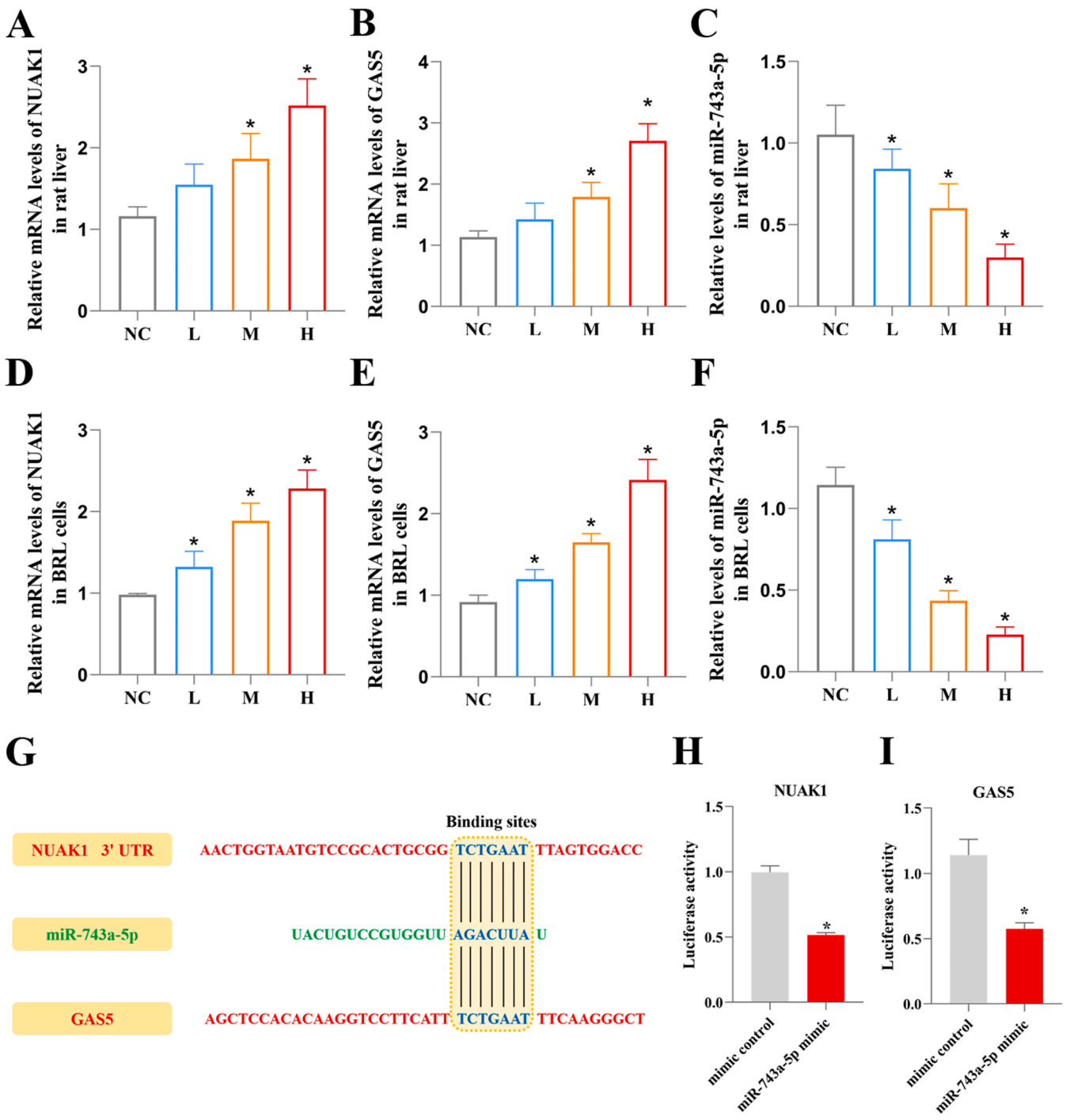

Fig. 4. Both NUAK1 and GAS5 are target genes for miR-743a-5p. (A) The mRNA level of NUAK1 in liver after BTBPE exposure. (B) The relative level of GAS5 in liver after BTBPE exposure. (C) The relative level of miR-743a-5p in liver after BTBPE exposure. (D) The mRNA level of NUAK1 in BRL cells after BTBPE exposure. (E) The relative level of GAS5 in BRL cells after BTBPE exposure. (F) The relative level of miR-743a-5p in BRL cells after BTBPE exposure. (G) The binding sites of miR-743a-5p in 3′UTR of NUAK1 and GAS5 analyzed using bioinformatics methods. (H) Using dual luciferase reporter genes to determine the targeting relationship between 3′UTR of NUAK1 and miR-743a-5p. (I) Using dual luciferase reporter genes to determine the targeting relationship between GAS5 and miR-743a-5p. All experiments were repeated at least three times ($n \geq 3$). Results are expressed as mean ± standard deviation. The asterisk represents a significant difference compared to the NC group or between different groups (*$P < 0.05$).

calcium ions and ROS in the miR-743a-5p mimic+BTBPE group were significantly reduced. These results indicated that the miR-743a-5p mimic inhibited BTBPE-induced necroptosis in BRL cells, as well as the accompanying increase in cytoplasmic calcium ions and ROS levels. Thus, miR-743a-5p inhibits necroptosis through the targeted binding and inhibition of NUAK1.

3.7. GAS5 knockdown alleviates BTBPE-induced necroptosis in BRL cells

To investigate the mechanism of action of non-coding RNA GAS5 in BTBPE-induced necroptosis, we knocked down GAS5(si-GAS5) in BRL cells. As shown in Fig. 7A, BTBPE increased the level of GAS5 in cells. Compared to the BTBPE group, the expression level of GAS5 in the si-GAS5 +BTBPE group was significantly reduced, indicating that GAS5

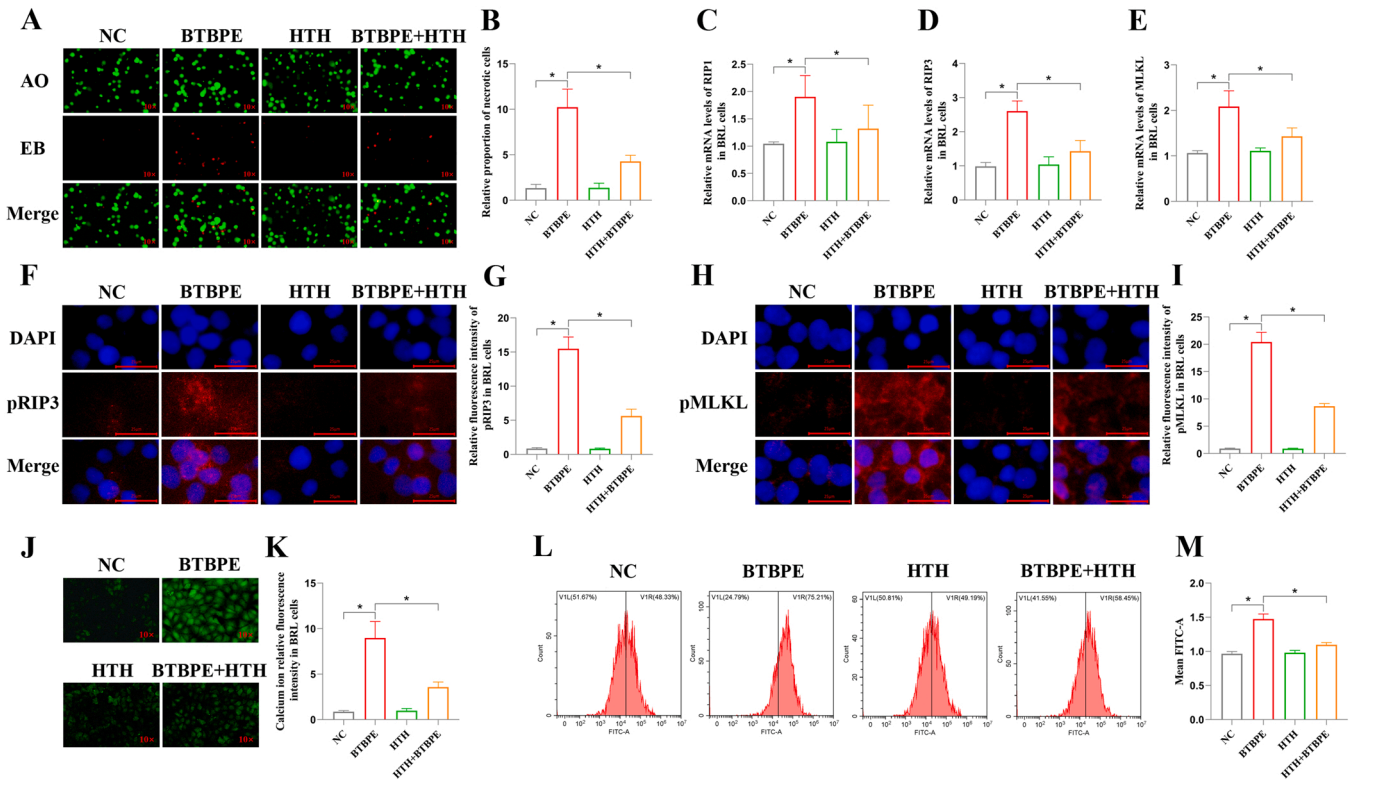

Fig. 5. NUAK1 inhibition alleviated necroptosis induced by BTBPE in BRL cells. (A) Effects of BTBPE and/or HTH on BRL cells necrosis by AO/EB staining. After AO/EB staining, the normal cells appeared green, and the necrotic cells appeared orange or orange-red. (B) Relative proportion of necrotic cells after BTBPE and/or HTH treatment. (C) The mRNA level of RIP1 in BRL cells after BTBPE and/or HTH treatment. (D) The mRNA level of RIP3 in BRL cells after BTBPE and/or HTH treatment. (E) The mRNA level of MLKL in BRL cells after BTBPE and/or HTH treatment. (F) Effects of BTBPE and/or HTH on protein level of pRIP3 in BRL cells analyzed using immunofluorescence. (G) pRIP3 relative fluorescence intensity after BTBPE and/or HTH treatment in BRL cells. (H) Effects of BTBPE and/or HTH on protein level of pMLKL in BRL cells analyzed using immunofluorescence. (I) pMLKL relative fluorescence intensity after BTBPE and/or HTH treatment in BRL cells. (J) Effects of BTBPE and/or HTH on level of cytoplasmic calcium ion in BRL cells analyzed using a Fluo-4 probe. (K) Cytoplasmic calcium ion relative fluorescence intensity after BTBPE and/or HTH treatment in BRL cells. (L) Effects of BTBPE and/or HTH on level of ROS in BRL cells analyzed using a DCFH probe. (M) ROS relative level in BRL cells after BTBPE and/or HTH treatment. All experiments were repeated at least three times ($n \geq 3$). Results are expressed as mean ± standard deviation. The asterisk represents a significant difference compared to the NC group or between different groups ($*P < 0.05$).

was effectively inhibited by si-GAS5. First, AO/EB staining showed that compared with the NC group, the proportion of necrotic cells in the BTBPE group was significantly increased, whereas in the si-GAS5 +BTBPE group, it was significantly decreased compared with the BTBPE group (Fig. 7B and C). Further experiments showed that si-GAS5 reduced the increased mRNA levels of RIP1, RIP3 and MLKL induced by BTBPE (Fig. 7D-F). Similarly, the BTBPE-induced increase in RIP1, pRIP3, and pMLKL protein levels was significantly inhibited by si-GAS5 (Fig. 3C and D, Fig. 7G and H, and Fig. 7I and J). Then, cytoplasmic calcium ions and ROS levels were measured (Fig. 7K-N). Cytoplasmic calcium ion and ROS levels in the BTBPE group were significantly higher than those in the NC group. Compared to the BTBPE group, the levels of cytoplasmic calcium ions and ROS in the si-GAS5 +BTBPE group were reduced. These results indicate that GAS5 knockdown inhibits BTBPE-induced necroptosis, as well as the accompanying increase in cytoplasmic calcium ions and ROS levels. Thus, GAS5 is involved in necroptosis regulation.

3.8. The contribution of NUAK1 to necroptosis is mitigated by miR-743a-5p

To explore the interaction between NUAK1 and miR-743a-5p during necroptosis, we overexpressed NUAK1 (OE-NUAK1) in BRL cells. In cells transfected with a recombinant plasmid containing the gene sequence of NUAK1, the gene expression level of NUAK1 was significantly increased, whereas after adding the miR-743a-5p mimic, the gene expression level of NUAK1 was significantly reduced (Fig. 4A). The AO/EB staining results showed that the proportion of necrotic cells in the OE-NUAK1 group was significantly higher than that in the NC group, and that in the miR-743a-5p mimic+OE-NUAK1 group was significantly lower than that in the OE-NUAK1 group (Fig. 4B and C). Further experiments showed that the miR-743a-5p mimic reduced the increased gene expression levels of RIP1, RIP3, and MLKL mediated by OE-NUAK1 (Fig. 4D-F). Similarly, the increased protein levels of RIP1, pRIP3, and pMLKL induced by OE-NUAK1 were significantly inhibited by the miR-743a-5p mimic (Fig. 5A-B, SFig. 4 G and H, and SFig. 4I and J). Cytoplasmic calcium ion and ROS levels were also detected (Fig. 4K-N). The cytoplasmic calcium and ROS levels in the OE-NUAK1 group were significantly higher than those in the NC group. Cytoplasmic calcium ion and ROS levels in the miR-743a-5p mimic+OE-NUAK1 group were significantly lower than those in the OE-NUAK1 group. These results demonstrate that the miR-743a-5p mimic directly inhibited OE-NUAK1-mediated necroptosis in BRL cells.

3.9. The contribution of GAS5 to necroptosis is mitigated by miR-743a-5p

To directly explore the interaction between GAS5 and miR-743a-5p during necroptosis, we overexpressed GAS5 (OE-GAS5) in BRL cells. In cells transfected with the recombinant plasmid containing the GAS5 full-length sequence, the GAS5 gene expression level was significantly increased, whereas after adding the miR-743a-5p mimic, the GAS5 gene expression level was significantly reduced (Fig. 6A). After OE-GAS5 transfection, the transfection efficiency of miR-743a-5p mimic could be significantly inhibited, as shown in Fig. 6B. In addition, the

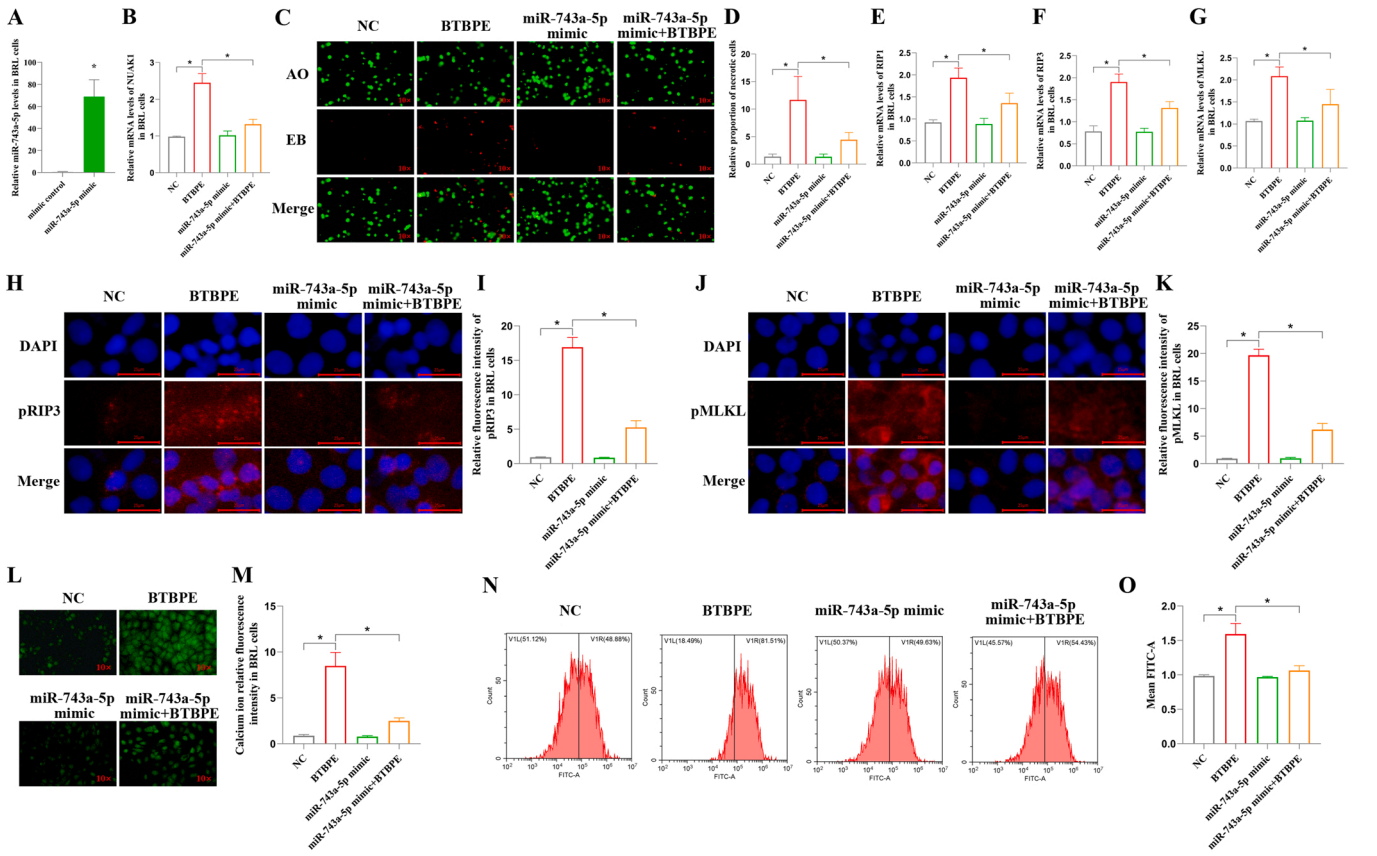

Fig. 6. miR-743a-5p alleviated necroptosis induced by BTBPE in BRL cells. (A) The relative level of miR-743a-5p in BRL cells after miR-743a-5p mimic treatment. (B) The mRNA level of NUAK1 in BRL cells after BTBPE and/or miR-743a-5p mimic treatment. (C) Effects of BTBPE and/or miR-743a-5p mimic on BRL cells necrosis analyzed using AO/EB staining. After AO/EB staining, the normal cells appeared green, and the necrotic cells appeared orange or orange-red. (D) Relative proportion of necrotic cells after BTBPE and/or miR-743a-5p mimic treatment. (E) The mRNA level of RIP1 in BRL cells after BTBPE and/or miR-743a-5p mimic treatment. (F) The mRNA level of RIP3 in BRL cells after BTBPE and/or miR-743a-5p mimic treatment. (G) The mRNA level of MLKL in BRL cells after BTBPE and/or miR-743a-5p mimic treatment. (H) Effects of BTBPE and/or miR-743a-5p mimic on protein level of pRIP3 in BRL cells analyzed using immunofluorescence. (I) pRIP3 relative fluorescence intensity after BTBPE and/or miR-743a-5p mimic treatment in BRL cells. (J) Effects of BTBPE and/or miR-743a-5p mimic on protein level of pMLKL in BRL cells analyzed using immunofluorescence. (K) pMLKL relative fluorescence intensity after BTBPE and/or miR-743a-5p mimic treatment in BRL cells. (L) Effects of BTBPE and/or miR-743a-5p mimic on level of cytoplasmic calcium ion in BRL cells analyzed using a Fluo-4 probe. (M) Cytoplasmic calcium ion relative fluorescence intensity after BTBPE and/or miR-743a-5p mimic treatment in BRL cells. (N) Effects of BTBPE and/or miR-743a-5p mimic on level of ROS in BRL cells analyzed using a DCFH probe. (O) ROS relative level in BRL cells after BTBPE and/or miR-743a-5p mimic treatment. All experiments were repeated at least three times ($n \geq 3$). Results are expressed as mean ± standard deviation. The asterisk represents a significant difference compared to the NC group or between different groups ($*P < 0.05$).

expression of NUAK1 in the OE-GAS5 group was significantly higher than that in the control group, and the expression of NUAK1 in the miR-743a-5p mimic+OE-GAS5 group was significantly lower than that in the OE-GAS5 group (Fig. 6C). This indicates that GAS5 can effectively consume miR-743a-5p, thereby increasing the expression level of NUAK1. Overexpression of miR-743a-5p effectively inhibited the elevation in NUAK1 induced by OE-GAS5. Therefore, the GAS5-miR-743a-5p-NUAK1 axis was established.

AO/EB staining showed that the proportion of necrotic cells in the OE-GAS5 group was significantly higher than that in the NC group, and that in the miR-743a-5p mimic+OE-GAS5 group was significantly lower than that in the OE-GAS5 group (Fig. 7A and B). Further experiments showed that the miR-743a-5p mimic reduced the increased gene expression levels of RIP1, RIP3, and MLKL mediated by OE-GAS5 (Fig. 7C-E). Similarly, the increased protein levels of RIP1, pRIP3, and pMLKL induced by OE-GAS5 were significantly inhibited by the miR-743a-5p mimic (Fig. 5C-D, SFig. 7F and G, and SFig. 7H and I). Then, cytoplasmic calcium ion and ROS levels were also measured (Fig. 7J-M). The cytoplasmic calcium and ROS levels in the OE-GAS5 group were significantly higher than those in the NC group. The levels of cytoplasmic calcium ions and ROS in the miR-743a-5p mimic+OE-GAS5 group were significantly lower than those in the OE-GAS5 group. These results showed that the miR-743a-5p mimic directly inhibited OE-GAS5-mediated necroptosis in BRL cells. Thus, the GAS5-miR-743a-5p-NUAK1 axis is involved in necroptosis regulation.

4. Discussion

Necroptosis is a type of inflammatory cell death [38]. We found that BTBPE exposure causes hepatitis, and our previous study showed that BTBPE can induce necroptosis in the intestine[12]. Therefore, we studies hepatocyte necroptosis, which was experimentally confirmed. Different forms of programmed cell death have different markers, and are associated with different biological effects. Necroptosis, as a form of programmed cell death, is characterized by the expression levels of RIP1, RIP3, and MLKL proteins and their phosphorylated proteins, accompanied by elevated levels of intracellular ROS and calcium ions [17,19,39]. Necroptosis can cause inflammation because of the extravasation of cellular contents in vivo [12]. In our study, BTBPE exposure increased the expression levels of RIP1, RIP3, and MLKL in the liver and hepatocytes, protein expression levels of RIP1, pRIP3, and pMLKL in hepatocytes, ROS and cytoplasmic calcium ion levels in BRL cells, and

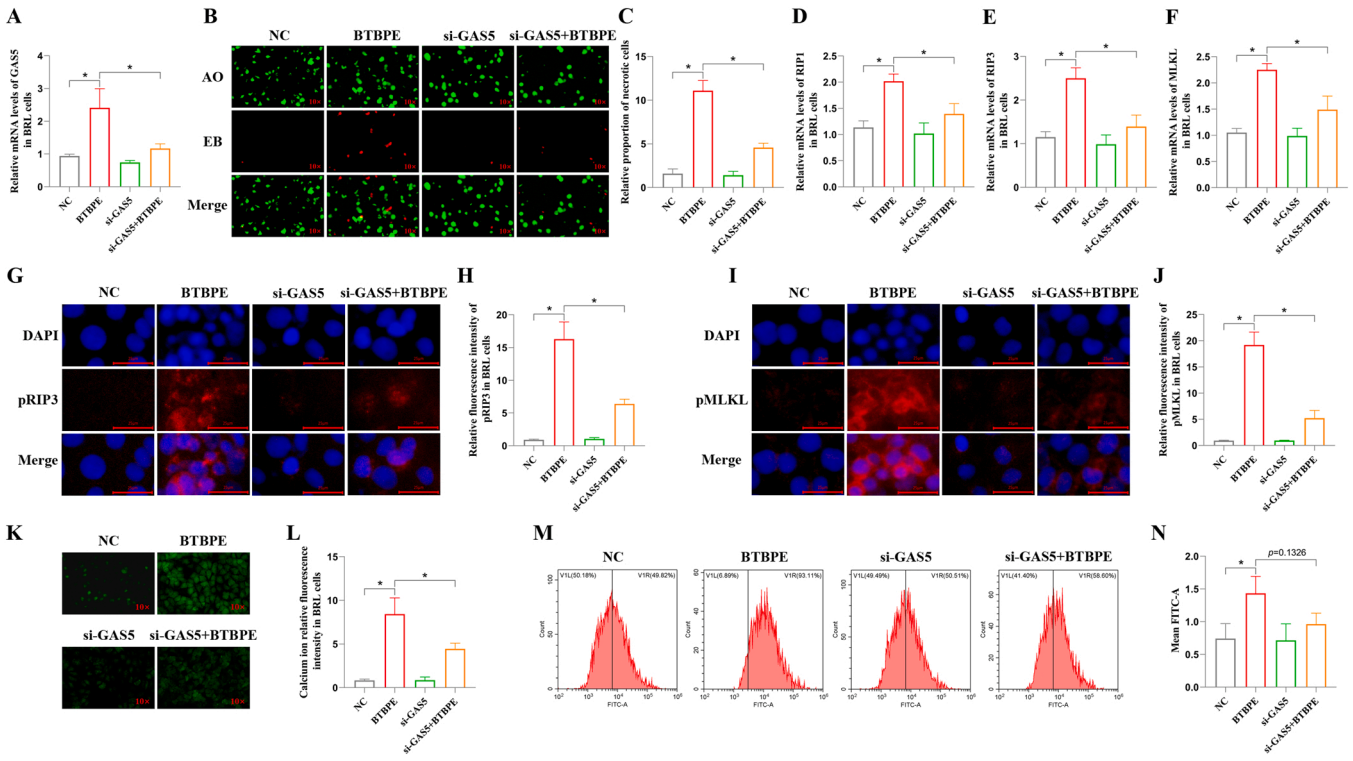

Fig. 7. GAS5 knockdown alleviated BTBPE-induced necroptosis in BRL cells. (A) The relative level of GAS5 in BRL cells after BTBPE and/or si-GAS5 treatment. (B) Effects of BTBPE and/or si-GAS5 on BRL cells necrosis by AO/EB staining. After AO/EB staining, the normal cells appeared green, and the necrotic cells appeared orange or orange-red. (C) Relative proportion of necrotic cells after BTBPE and/or si-GAS5 treatment. (D) The mRNA level of RIP1 in BRL cells after BTBPE and/or si-GAS5 treatment. (E) The mRNA level of RIP3 in BRL cells after BTBPE and/or si-GAS5 treatment. (F) The mRNA level of MLKL in BRL cells after BTBPE and/or si-GAS5 treatment. (G) Effects of BTBPE and/or si-GAS5 on protein level of pRIP3 in BRL cells analyzed using immunofluorescence. (H) pRIP3 relative fluorescence intensity after BTBPE and/or si-GAS5 treatment in BRL cells. (I) Effects of BTBPE and/or si-GAS5 on protein level of pMLKL in BRL cells analyzed using immunofluorescence. (J) pMLKL relative fluorescence intensity after BTBPE and/or si-GAS5 treatment in BRL cells. (K) Effects of BTBPE and/or si-GAS5 on level of cytoplasmic calcium ion in BRL cells analyzed using a Fluo-4 probe. (L) Cytoplasmic calcium ion relative fluorescence intensity after BTBPE and/or si-GAS5 treatment in BRL cells. (M) Effects of BTBPE and/or si-GAS5 on level of ROS in BRL cells analyzed using a DCFH probe. (N) ROS relative level in BRL cells after BTBPE and/or si-GAS5 treatment. All experiments were repeated at least three times (n $\geq$ 3). Results are expressed as mean $\pm$ standard deviation. The asterisk represents a significant difference compared to the NC group or between different groups (*$P < 0.05$).

inflammatory responses in the liver. These studies indicated that BTBPE has a necroptotic effect on hepatocytes.

Currently, the research on NUAK1 is limited. To investigate the biological effects of NUAK1 on hepatocytes, we knocked down NUAK1. HTH is a commercialized NUAK1-specific inhibitor. The inhibitory effect of HTH on NUAK1 is more than 100 times higher than that on NUAK2 [40]. Therefore, compared to other NUAK1 inhibitors, HTH was more suitable for our study. In our study, we found that after BTBPE exposure, the gene expression levels of NUAK1 in the liver and BRL cells increased significantly, and the use of NUAK1 specific inhibitors reduced BTBPE-induced necroptosis. Further experiments demonstrated that NUAK1 overexpression in BRL cells can also cause necroptosis, suggesting that NUAK1 may be an upstream regulator of necroptosis. Additionally, we focused on another target, lncRNA GAS5 [41,42]. However, whether there is a link between GAS5 and necroptosis has not been investigated. In our study, we found that GAS5 expression levels in the liver and BRL cells were significantly elevated after BTBPE exposure and that interfering with GAS5 with siRNA reduced BTBPE-induced necroptosis. We demonstrated that the overexpression of GAS5 in BRL cells can also cause necroptosis. These results indicate that GAS5 is also involved in the regulation of necroptosis.

Next, we explored the relationship between NUAK1, GAS5, and necroptosis. In the present study, overexpression and inhibition of NUAK1 regulated necroptosis, suggesting that NUAK1 plays a role in the regulation of necroptosis. It is worth noting that GAS5, as a non-coding RNA, cannot be translated into proteins, so GAS5 usually acts as an RNA [41,43–45]. Bioinformatics analysis revealed that NUAK1 and GAS5 share a common target miRNA, miR-743a-5p. In vitro and in vivo studies showed that the expression of miR-743a-5p was significantly reduced after BTBPE treatment. This is in contrast to the expression trends of NUAK1 and GAS5, which attracted our interest. A dual-luciferase reporter gene assay showed that NUAK1 and GAS5 target miR-743a-5p. This led us to investigate their relationship with necroptosis from the ceRNA perspective [46,47].

After treating BRL cells with a miR-743a-5p mimic, we found that miR-743a-5p inhibited necroptosis caused by BTBPE by inhibiting NUAK1. This suggests that the miR-743a-5p-NUAK1 axis is involved in the regulation of necroptosis. Subsequently, after overexpression of GAS5, we found that the level of miR-743a-5p was reduced and that of NUAK1 was increased. In addition, necroptosis caused by NUAK1 and GAS5 overexpression was significantly inhibited by the miR-743a-5p mimic. These results indicated that the GAS5-miR-743a-5p-NUAK1 axis is involved in the regulation of necroptosis in the form of a ceRNA. Thus, GAS5 and NUAK1 induce necroptosis by co-competing with miR-743a-5p. In addition, the correlation analysis results showed that GAS5 and NUAK1 were significantly positively correlated with necroptosis-related genes, whereas miR-743a-5p was significantly negatively correlated with necroptosis-related genes, which also supports our hypothesis.

One limitation of this study is that the in vitro mechanism has not been validated in vivo. Subsequent research should validate the mechanisms discovered in this study in vivo using pharmacological and gene

editing methods as well as verify whether the GAS5-miR-743a-5p-NUAK1 axis regulates necroptosis on various other necroptosis models.

5. Conclusion

In summary, our study found that BTBPE exposure caused necroptosis in the liver and BRL cells, accompanied by an oxidation-reduction imbalance. Importantly, NUAK1 is a newly discovered upstream regulatory target for necroptosis. In addition, miR-743a-5p was shown for the first time to inhibit necroptosis by targeting NUAK1 and down-regulating NUAK1. GAS5 upregulates NUAK1 expression by competitively binding to miR-743a-5p, thereby inducing necroptosis. Thus, GAS5 and NUAK1 induce necroptosis by competitively binding to miR-743a-5p.

Environmental implication

The brominated flame retardant BTBPE widelyused in manufacturing is inevitably released into the environment, resulting inthe exposure of organisms toBTBPE; therefore, it is particularly important toexplore its toxic mechanism. The liver is one of the main accumulating organsof BTBPE; however, the mechanism underlying BTBPE hepatotoxicity has not beenthoroughly investigated. Our study is the first to explore the mechanism ofhepatotoxicity fromthe perspective of ceRNA caused by BTBPE exposure. We discovered that theGAS5-miR-743a-5p-NUAK1 axis is involved in the occurrence of necroptosis.

CRediT authorship contribution statement

Qianqian Xiao: Methodology, Formal analysis. **Yuan Cui:** Writing – original draft, Visualization, Conceptualization. **Jianjun Jiang:** Supervision, Project administration. **Weidong Hao:** Resources. **Xuetao Wei:** Funding acquisition. **Qinghe Meng:** Supervision, Project administration. **Yuetong Liu:** Methodology, Formal analysis. **Jiawei Yang:** Data curation. **Qiong Zhang:** Data curation.

Declaration of Competing Interest

The authors declare that they have no known competing financial interests or personal relationships that could have appeared to influence the work reported in this paper.

Data Availability

Data will be made available on request.

Acknowledgements

The study was supported by the Major Special Project of Agricultural Biological Breeding for No. 2023ZD0406302.

Appendix A. Supporting information

Supplementary data associated with this article can be found in the online version at doi:10.1016/j.jhazmat.2024.135375.

References

[1] Fromme, H., Becher, G., Hilger, B., Völkel, W., 2016. Brominated flame retardants - exposure and risk assessment for the general population. Int J Hyg Environ Health 219, 1–23.
[2] de Jourdan, B.P., Hanson, M.L., Muir, D.C.G., Solomon, K.R., 2014. Fathead minnow (Pimephales promelas RAFINESQUE) exposure to three novel brominated flame retardants in outdoor mesocosms: bioaccumulation and biotransformation. Environ Toxicol Chem 33, 1148–1155.
[3] Shanmuganathan, M., Zhang, Z.F., Sverko, E., Brymer, R., Gill, B., Smyth, S., et al., 2018. Analysis of halogenated flame retardants in Canadian wastewater treatment plants using gas chromatography-tandem mass spectrometry (GC-MS/MS). Water Qual Res J Canada 53, 167–180.
[4] Lee, H.K., Kang, H., Lee, S., Kim, S., Choi, K., Moon, H.B., 2020. Human exposure to legacy and emerging flame retardants in indoor dust: a multiple-exposure assessment of PBDEs. Sci Total Environ 719, 9.
[5] Covaci, A., Harrad, S., Abdallah, M.A.E., Ali, N., Law, R.J., Herzke, D., et al., 2011. Novel brominated flame retardants: a review of their analysis, environmental fate and behaviour. Environ Int 37, 532–556.
[6] Chen, T., Yu, D., Yang, L.P., Sui, S.F., Lv, S.B., Bai, Y., et al., 2019. Thyroid function and decabromodiphenyl ethane (DBDPE) exposure in Chinese adults from a DBDPE manufacturing area. Environ Int 133, 8.
[7] Giraudo, M., Douville, M., Letcherb, R.J., Houde, M., 2017. Effects of food-borne exposure of juvenile rainbow trout (Oncorhynchus mykiss) to emerging brominated flame retardants 1,2-bis(2,4,6-tribromophenoxy)ethane and 2-ethylhexyl-2,3,4,5-tetrabromobenzoate. Aquat Toxicol 186, 40–49.
[8] Shi, J., Wang, X.T., Chen, L.L., Deng, H.P., Zhang, M., 2021. HBCD, TBECH, and BTBPE exhibit cytotoxic effects in human vascular endothelial cells by regulating mitochondria function and ROS production. Environ Toxicol 36, 1674–1682.
[9] Choi, J., Lee, G., Kim, S., Choi, K., 2021. Investigation on sex hormone-disruption effects of two novel brominated flame retardants (DBDPE and BTBPE) in Male Zebrafish (Danio rerio) and two human cell lines (H295R and MVLN). Appl Sci 11, 12.
[10] Smythe, T.A., Butt, C.M., Stapleton, H.M., Pleskach, K., Ratnayake, G., Song, C.Y., et al., 2017. Impacts of unregulated novel brominated flame retardants on human liver thyroid deiodination and sulfotransferation. Environ Sci Technol 51, 7245–7253.
[11] Zhang, Q., Wang, Z.Y., Xiao, Q.Q., Ge, J.H., Wang, X.Y., Jiang, W.Y., et al., 2023. The effects and mechanisms of the new brominated flame retardant BTBPE on thyroid toxicity. Food Chem Toxicol 180, 10.
[12] Cui, Y., Xiao, Q.Q., Wang, Z.Y., Zhang, Q., Liu, Y.T., Hao, W.D., et al., 2024. 1,2-bis (2,4,6-tribromophenoxy) ethane, a novel brominated flame retardant, disrupts intestinal barrier function via the IRX3/NOS2 axis Rat small Intest. J Hazard Mater 461, 13.
[13] Nano, M., Montell, D.J., 2024. Apoptotic signaling: beyond cell death. Semin Cell Dev Biol 156, 22–34.
[14] Xu, T., Liu, Q.H., Chen, D., Liu, Y.Y., 2022. Atrazine exposure induces necroptosis through the P450/ROS pathway and causes inflammation in the gill of common carp (Cyprinus carpio L.). Fish Shellfish Immunol 131, 809–816.
[15] Miao, Z.Y., Miao, Z.R., Teng, X.H., Xu, S.W., 2022. Melatonin alleviates lead-induced intestinal epithelial cell pyroptosis in the common carps (Cyprinus carpio) via miR-17-5p/TXNIP axis. Fish Shellfish Immunol 131, 127–136.
[16] Yin, K., Wang, D.X., Zhao, H.J., Wang, Y., Zhang, Y., Liu, Y.C., et al., 2022. Polystyrene microplastics up-regulates liver glutamine and glutamate synthesis and promotes autophagy-dependent ferroptosis and apoptosis in the cerebellum through the liver-brain axis. Environ Pollut 307, 12.
[17] Cui, Y., Xiao, Q.Q., Yuan, Y.S., Zhuang, Y.M., Hao, W.D., Jiang, J.J., et al., 2023. 1,4-Naphthoquinone-coated black carbon, a kind of atmospheric fine particulate matter, affects macrophage fate: new insights into crosstalk between necroptosis and macrophage extracellular traps. Environ Sci Technol 57, 6095–6107.
[18] Cui, Y., Xiao, Q.Q., Yuan, Y.S., Zhuang, Y.M., Hao, W.D., Jiang, J.J., et al., 2023. Ozone-oxidized black carbon particles change macrophage fate: crosstalk between necroptosis and macrophage extracellular traps. Environ Pollut 329, 12.
[19] Cui, Y., Xiao, Q.Q., Zhang, Q., Liu, Y.T., Hao, W.D., Jiang, J.J., et al., 2023. Black carbon nanoparticles activate the crosstalk mechanism between necroptosis and macrophage extracellular traps to change macrophages fate. Environ Res 232, 10.
[20] Courchet, J., Lewis, T.L., Lee, S., Courchet, V., Liou, D.Y., Aizawa, S., et al., 2013. Terminal axon branching is regulated by the LKB1-NUAK1 Kinase pathway via presynaptic mitochondrial capture. Cell 153, 1510–1525.
[21] Liu, L.D., Ulbrich, J., Müller, J., Wüstefeld, T., Aeberhard, L., Kress, T.R., et al., 2012. Deregulated MYC expression induces dependence upon AMPK-related kinase 5. Nature 483, 608–U131.
[22] Zagórska, A., Deak, M., Campbell, D.G., Banerjee, S., Hirano, M., Aizawa, S., et al., 2010. New roles for the LKB1-NUAK pathway in controlling myosin phosphatase complexes and cell adhesion. Sci Signal 3, 13.
[23] Humbert, N., Navaratnam, N., Augert, A., Da Costa, M., Martien, S., Wang, J., et al., 2010. Regulation of ploidy and senescence by the AMPK-related kinase NUAK1. Embo J 29, 376–386.
[24] Hou, X., Liu, J.E., Liu, W., Liu, C.Y., Liu, Z.Y., Sun, Z.Y., 2011. A new role of NUAK1: directly phosphorylating p53 and regulating cell proliferation. Oncogene 30, 2933–2942.
[25] Al-Hakim, A.K., Zagorska, A., Chapman, L., Deak, M., Peggie, M., Alessi, D.R., 2008. Control of AMPK-related kinases by USP9X and atypical Lys²⁹/Lys³³-inked polyubiquitin chains. Biochem J 411, 249–260.
[26] Tay, Y., Rinn, J., Pandolfi, P.P., 2014. The multilayered complexity of ceRNA crosstalk and competition. Nature 505, 344–352.
[27] St Laurent, G., Wahlestedt, C., Kapranov, P., 2015. The Landscape of long noncoding RNA classification. Trends Genet 31, 239–251.
[28] Wang, K.C., Chang, H.Y., 2011. Molecular mechanisms of long noncoding RNAs. Mol Cell 43, 904–914.
[29] Fatica, A., Bozzoni, I., 2014. Long non-coding RNAs: new players in cell differentiation and development. Nat Rev Genet 15, 7–21.
[30] Flynn, R.A., Chang, H.Y., 2014. Long noncoding RNAs in cell-fate programming and reprogramming. Cell Stem Cell 14, 752–761.
[31] Ala, U., 2020. Competing endogenous RNAs, non-coding RNAs and diseases: an intertwined story. Cells 9, 23.

[32] Song, N., Li, X.J., Cui, Y., Zhang, T.Y., Xu, S.W., Li, S., 2021. Hydrogen sulfide exposure induces pyroptosis in the trachea of broilers via the regulatory effect of circRNA-17828/miR-6631-5p/DUSP6 crosstalk on ROS production☆. J Hazard Mater 418, 14.
[33] Wang, Y.Y., Luo, W.K., Tang, S.X., Xiang, J., Dang, Y., Tang, B., et al., 2024. Bioaccumulation and biotransformation of 1,2-bis (2,4,6-tribromophenoxyethane) (BTBPE) and 1,2-dibromo-4-(1,2-dibromoethyl)-cyclohexane (TBECH) in zebrafish (Danio rerio). In: Environmental pollution, 345, 123460.
[34] Sun, W., Lei, Y., Jiang, Z., Wang, K., Liu, H., Xu, T., 2024. BPA and low-Se exacerbate apoptosis and mitophagy in chicken pancreatic cells by regulating the PTEN/PI3K/AKT/mTOR pathway. J Adv Res.
[35] Li, S.S., Gu, X.D., Zhang, M.Y., Jiang, Q.H., Xu, T., 2024. Di (2-ethylhexyl) phthalate and polystyrene microplastics co-exposure caused oxidative stress to activate NF-κB/NLRP3 pathway aggravated pyroptosis and inflammation in mouse kidney. Sci Total Environ 926, 12.
[36] Shi, X., Xu, T., Gao, M.C., Bi, Y.J., Wang, J.Q., Yin, Y.L., et al., 2024. Combined exposure of emamectin benzoate and microplastics induces tight junction disorder, immune disorder and inflammation in carp midgut via lysosome/ROS/ferroptosis pathway. Water Res 257, 14.
[37] Lv, X.A., Ren, M.Y., Xu, T., Gao, M.C., Liu, H.Y., Lin, H.J., 2023. Selenium alleviates lead-induced CIK cells pyroptosis and inflammation through IRAK1/TAK1/IKK pathway. Fish Shellfish Immunol 142, 8.
[38] Lei, Y.T., Xu, T., Sun, W.Y., Wang, X.D., Gao, M.C., Lin, H.J., 2023. Evodiamine alleviates DEHP-induced hepatocyte pyroptosis, necroptosis and immunosuppression in grass carp through ROS-regulated TLR4/MyD88/NF-κB pathway. Fish Shellfish Immunol 140, 9.
[39] Cui, Y., Yin, K., Gong, Y.Z., Qu, Y.Y., Liu, H.G., Lin, H.J., 2019. Atrazine induces necroptosis by miR-181-5p targeting inflammation and glycometabolism in carp lymphocytes. Fish Shellfish Immunol 94, 730–738.
[40] Banerjee, S., Buhrlage, S.J., Huang, H.T., Deng, X.M., Zhou, W.J., Wang, J.H., et al., 2014. Characterization of WZ4003 and HTH-01-015 as selective inhibitors of the LKB1-tumour-suppressor-activated NUAK kinases. Biochem J 457, 215–225.
[41] Sun, M., Jin, F.Y., Xia, R., Kong, R., Li, J.H., Xu, T.P., et al., 2014. Decreased expression of long noncoding RNA GAS5 indicates a poor prognosis and promotes cell proliferation in gastric cancer. BMC Cancer 14, 12.
[42] Ni, W., Yao, S., Zhou, Y.X., Liu, Y.Y., Huang, P., Zhou, A.J., et al., 2019. Long noncoding RNA GAS5 inhibits progression of colorectal cancer by interacting with and triggering YAP phosphorylation and degradation and is negatively regulated by the m⁶A reader YTHDF3. Mol Cancer 18, 20.
[43] Pickard, M.R., Mourtada-Maarabouni, M., Williams, G.T., 2013. Long non-coding RNA GAS5 regulates apoptosis in prostate cancer cell lines. Biochim Biophys Acta-Mol Basis Dis 1832, 1613–1623.
[44] Shi, X.F., Sun, M., Liu, H.B., Yao, Y.W., Kong, R., Chen, F.F., et al., 2015. A critical role for the long non-coding RNA GAS5 in proliferation and apoptosis in non-small-cell lung cancer. Mol Carcinog 54, E1–E12.
[45] Chen, L., Yang, W.J., Guo, Y.J., Chen, W., Zheng, P., Zeng, J.S., et al., 2017. Exosomal lncRNA GAS5 regulates the apoptosis of macrophages and vascular endothelial cells in atherosclerosis. PLoS One 12, 10.
[46] Denzler, R., Agarwal, V., Stefano, J., Bartel, D.P., Stoffel, M., 2014. Assessing the ceRNA hypothesis with quantitative measurements of miRNA and target abundance. Mol Cell 54, 766–776.
[47] Thomson, D.W., Dinger, M.E., 2016. Endogenous microRNA sponges: evidence and controversy. Nat Rev Genet 17, 272–283.